This is a author version of
David Schlipf, "Prospects of Multivariable Feedforward Control of Wind Turbines Using Lidar,"
published in Proceedings of the American Control Conference, Boston, MA, USA, 2016.

Prospects of Multivariable Feedforward Control of Wind Turbines Using Lidar

David Schlipf

***Abstract*— Current advances in lidar-technology provide the possibility of including wind preview information in the control design. Lidar-assisted collective pitch control is a simple, but promising approach to reduce the rotor speed variation and structural loads for full load operation. This work extends this approach to the transition between partial and full load operations. A multivariable controller is presented, which provides a simple update for the generator torque rate and the minimum pitch angle based on a nonlinear system inversion. The feedforward signals of the generator torque rate and the minimum pitch angle can be combined with conventional feedback controllers and the collective pitch feedforward controller for full load operation. This facilitates the modular application on commercial wind turbines. Simulations with a full aero-elastic wind turbine model and a lidar simulator show improved rotor speed regulation and significant reduction of tower loads, while only slightly decreasing power. Further, possibilities to transform the load reduction into energy increase are outlined.**

I. Introduction

Lidar-assisted control has become an important research topic in the wind turbine control community. During initial field testing, collective pitch feedforward control was able to reduce the rotor speed variation and structural loads during full load operation in several field tests, e.g. [1]-[4]. During partial load operation, lidar-assisted torque control shows only marginal benefit on power production while having negative impact on structural loads [5], [6]. Nonlinear model predictive control (NMPC) using only the collective pitch provides similar performance to collective pitch feedforward control during full load operation [7], but shows improved performance in the transition between partial and full load operations using additionally the generator torque [8]. Although NMPC is becoming computationally more effective [9], replacing the feedback controller makes it less attractive to turbine manufacturers. The flatness-based approach allows the calculation of the control action based on trajectories of the rotor speed and tower motion and also shows improved control performance in the transition region, but is difficult to tune [10]. In this work, an alternative is proposed, which can be more easily applied and still shows significant improvements.

This paper is organized as follows. Section II and III present the modeling of the wind turbines and the lidar measurements. In Section IV, the feedforward controller is designed, Section V provides the simulation results, and Section VI presents the conclusions and future work.

David Schlipf is with the Stuttgart Wind Energy (SWE) @ Institute of Aircraft Design, University of Stuttgart, Germany, David.Schlipf@ifb.uni-stuttgart.de.

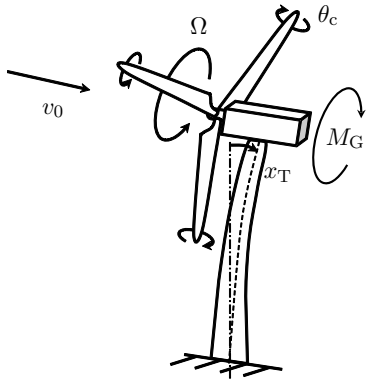

Fig. 1. Degrees of freedom for the reduced nonlinear model.

II. Modeling of the Wind Turbine

In this study, a full model of a 5 MW reference turbine [11] is used for simulations. A reduced version of the same turbine is used for the controller design.

A. Full Simulation Model

Simulations are done with the aero-elastic simulation tool FAST [12]. In FAST, an onshore wind turbine structure is modeled by a flexible multibody system, which experiences external forces from aerodynamics. The structural model represents dynamics of flexible parts such as the tower, blades, and drive train. The following 15 degrees of freedom (DOF) are enabled in the simulations: first and second flapwise modes and first edgewise mode of three blades, first and second side-to-side and fore-aft tower bending modes, rotor motion and drive train flexibility. Two different types of wind input files can be loaded to the aerodynamic subsystem. Coherent time series of wind characteristics such as wind speed, direction, and shears are used for the extreme load calculations in Section V-A. The fatigue simulations in Section V-B are done with a turbulent three-dimensional wind field over the rotor disk generated with TurbSim [13]. In both cases, aerodynamic forces along the blades are calculated iteratively by applying the Blade Element Momentum theory [14] and transferred to the structural model. The described simulation tools have proven to have reliable accuracy which justifies its application as a full simulation model in this work.

B. Reduced Controller Design Model

The aero-elastic model is not useful for controller design due to its complexity and the iterative calculation of the aerodynamics. Here, the SLOW (Simplified Low Order Wind

turbine) model from the flatness-based approach [10] is used with some minor changes. Similar to the full simulation model, SLOW consists of a reduced servo-elastic and aerodynamic module, see Figure 1.

In the servo-elastic part, only the first tower fore-aft bending mode and the rotational motion are considered:

$$J\dot{\Omega} + \frac{M_\mathrm{G}}{i_\mathrm{GB}} = M_\mathrm{a} \tag{1a}$$

$$m\ddot{x}_\mathrm{T} + c\dot{x}_\mathrm{T} + k(x_\mathrm{T} - x_\mathrm{0T}) = F_\mathrm{a}. \tag{1b}$$

Equation (1a) models the rotor dynamics, where Ω is the rotor speed, M_a is the aerodynamic torque and M_G the generator torque. Moreover, i_GB is the gearbox ratio and J is the overall sum of the moments of inertia of rotor and hub about the rotation axis. Equation (1b) describes the tower fore-aft dynamics, where F_a is the aerodynamic thrust, x_T the tower top fore-aft displacement, x_0T the static tower top fore-aft displacement, and m, c, and k are the tower equivalent modal mass, structural damping, and bending stiffness, respectively.

In the aerodynamic part, the aerodynamic torque and thrust acting on the rotor with the radius R are

$$M_\mathrm{a} = \frac{1}{2}\rho\pi R^3 \frac{c_\mathrm{P}(\lambda,\theta)}{\lambda} v_\mathrm{rel}^2 \tag{2a}$$

$$F_\mathrm{a} = \frac{1}{2}\rho\pi R^2 c_\mathrm{T}(\lambda,\theta) v_\mathrm{rel}^2, \tag{2b}$$

where ρ is the air density, λ the tip-speed ratio, defined as

$$\lambda = \frac{\Omega R}{v_\mathrm{rel}}, \tag{3}$$

and c_P and c_T are the effective power and thrust coefficients, respectively. Two dimensional look-up tables are used to obtain these coefficients, which are precalculated from steady state simulations with the full simulation model [15]. The relative wind speed v_rel is used to model the aerodynamic damping and is defined as the superposition of the tower top speed $\dot{x}_\mathrm{T}$ and the rotor effective wind speed v_0:

$$v_\mathrm{rel} = (v_0 - \dot{x}_\mathrm{T}). \tag{4}$$

III. Simulation of Lidar Measurements

For the lidar-assisted control of the collective pitch and generator torque, a preview of the rotor effective wind speed v_0 is necessary. Current lidar technology provides the possibility to measure the speed of aerosols in front of the turbine by back-scattered light. Due to limitations in the lidar measurements, only the lidar estimate of the rotor effective wind speed v_0L can be provided. Here, the same generic wind field applied to the aero-elastic simulation is scanned with a lidar simulator. The scan trajectory is optimized to provide the best coherence bandwidth for the measurements on the NREL 5 MW wind turbine based on [16].

Taylor's frozen turbulence hypothesis, which assumes that the turbulent wind field moves unaffected with the average wind speed, is used in the simulation of the measurements as well as for the wind speed estimation. Here, all measurements are condensed to the lidar estimate of the rotor effective wind speed v_0L. More details can be found in [15].

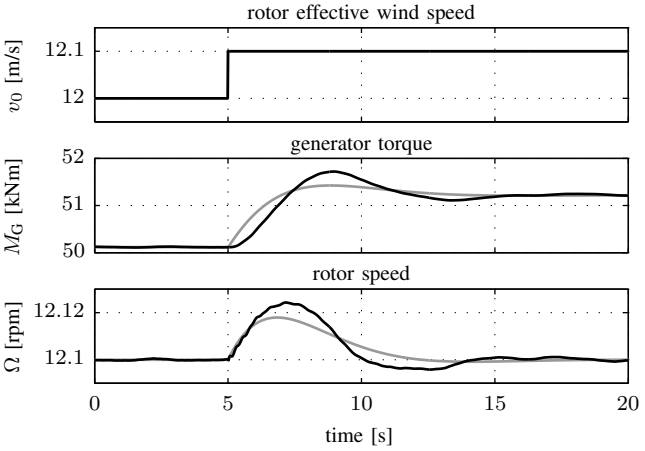

Fig. 2. Review of feedback controller design with a wind speed step. Desired behavior (gray) and full simulation model (black).

IV. Controller Design

In this section, the feedback controller for the transition region is designed. Then, the advantages and disadvantages of the flatness-based approach are discussed. Eventually, the lidar-assisted multivariable feedforward controller is derived for the cases of perfect and realistic wind preview.

A. Feedback Controller

In this work, only the transition (usually referred to as "region 2.5") between the operation of aerodynamic optimality ("region 2") and the full load operation ("region 3") is considered. The baseline feedback controller for the 5 MW reference wind turbine leaves region 2 at 10.3 m/s and $\Omega = 11.7$ rpm and then adjusts the generator torque M_G linearly with increasing rotational speed until reaching region 3 at 11.3 m/s and $\Omega_\mathrm{rated} = 12.1$ rpm [11].

However, commercial wind turbines often use a PI torque controller as proposed in [17]. The advantages are that the turbine can be operated with aerodynamic optimality over a larger range and the closed loop behavior can be tuned. The transition to region 2 is usually done by adjusting the lower limit of the torque PI controller using a optimal state feedback of region 2. Usually, a torque or power error term needs to be included in the pitch PI controller in addition to the speed error to have a smooth transition to region 3 and to prevent the pitch from acting during low wind speeds.

For this work, a generator torque feedback controller (FB) is designed by using the closed-loop-shaping method from the collective pitch controller design [18]. The rotor motion (1a) is linearized at 12 m/s and the proportional and integral gains are chosen, such that the closed loop from wind speed v_0 to generator speed $\Omega_\mathrm{G} = \Omega / i_\mathrm{GB}$ has a damping of 0.7 and a natural frequency of 0.6 rad/s. The response of the full simulation model to a wind speed step from 12 m/s to 12.1 m/s is close to the desired behavior, see Figure 2. The deviations are due to the generator torque filter and the dynamics neglected in the design approach.

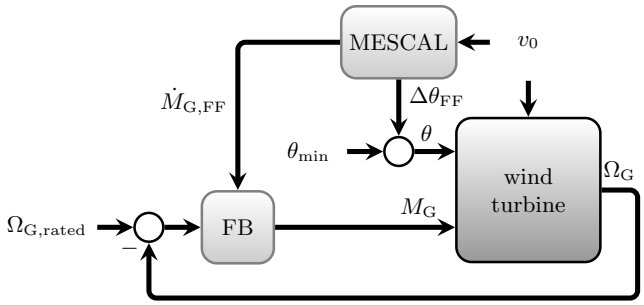

Fig. 3. Control loop with feedback and multivariable feedforward.

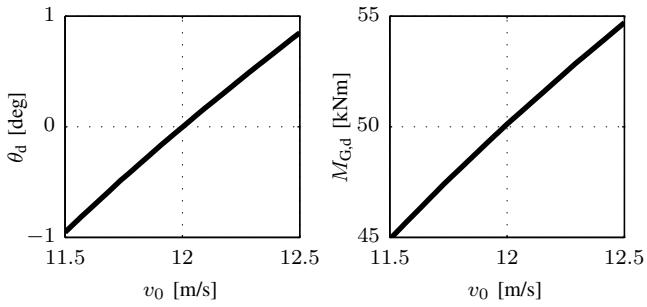

Fig. 4. Necessary pitch angle and generator torque to maintain the wind turbine in its steady state for wind speed deviations from 12 m/s.

The rated power is increased to 8 MW to have a sufficiently large region 2.5 (ranging now from 10.6 m/s to 13.6 m/s) to test the designed feedback and feedforward controller. Increasing the rated power of wind turbines of the same size while keeping the same rotor and rotor speed has been done by industry and thus seems to a realistic scenario[1].

The pitch feedback controller is not further considered in this paper, since all simulations are performed only in region 2.5, where the pitch angle is limited to $\theta_{\min} = 0\,\mathrm{deg}$.

Figure 3 shows the overall control loop.

B. Pros and Cons of the Flatness-Based Approach

A flatness-based feedforward controller has been introduced in [10]. Based on the wind speed preview and considering system constraints, trajectories of the rotor speed and tower motions are continuously designed during operation and with an inverse wind turbine model translated into trajectories for the pitch angle and the generator torque. The trajectories are planned to minimize the tower movements during the transition between partial and full load operations. The approach has the following advantages:

+ The feedforward controller is nonlinear and can be used in all regions without scheduling.
+ Tower and rotor motion are directly reduced by a feedforward of the pitch angle and generator torque.
+ It can be combined with a conventional feedback controller.
+ All feedforward signals have zero-mean and can be set to zero, if problems with the wind preview are detected.
+ Is computationally less expensive compared to NMPC.

However, there are also disadvantages compared to the collective pitch feedforward controller used in [1]-[4]:

– The trajectory planning for the rotor and tower motion is difficult to tune.
– Pitch angle and generator torque trajectories are not directly designed and might result in extreme inputs.
– The overall concept is quite complicated.

The feedforward controller presented in the next subsections lacks these disadvantages, but abandons the first advantage by linearizing and simplifying the flatness-based approach for the region 2.5. The other advantages can be maintained.

[1]The Senvion 6.2M126 with a rated power of 6.2 MW is based on the 5M with 5 MW. The rated power of the Enercon E-126 was increased from 6 MW to 7.6 MW. More details can be found on the company websites.

C. Multivariable Extension based on Simplified Calculations

The Multivariable Extension based on Simplified Calculations (MESCAL) is derived in three main steps:

1) Calculation of control actions.
2) Linearization and control actions.
3) Combination with feedback.

In the first step, the inverse model of the flatness-based controller is used to calculate the desired generator torque and pitch angle to mitigate the effect of changes in the rotor effective wind speed v_0 to the rotor and tower motion for a given operating point. In contrast to the flatness-based feedforward controller, no dynamics for the rotor and tower motion are designed ($\dot{\Omega}_{\mathrm{d}} = \dot{x}_{\mathrm{T,d}} = \ddot{x}_{\mathrm{T,d}} = 0$). With the desired rotor speed $\Omega_{\mathrm{d}} = \Omega_{\mathrm{rated}}$ and using (3), the desired tip speed ratio λ_{d} is

$$\lambda_{\mathrm{d}} = \frac{\Omega_{\mathrm{d}} R}{v_0}. \tag{5}$$

With the desired tower top displacement $x_{\mathrm{T,d}}$ and using (1b) and (2b), the desired thrust coefficient is

$$c_{\mathrm{T,d}} = \frac{2F_{\mathrm{a,d}}}{\rho\pi R^2 v_0^2} \text{ with } F_{\mathrm{a,d}} = k(x_{\mathrm{T,d}} - x_{0\mathrm{T}}). \tag{6}$$

Using a inverse $\theta(\lambda, c_{\mathrm{T}})$ of the look-up table $c_{\mathrm{T}}(\lambda, \theta)$, one obtains the desired pitch angle

$$\theta_{\mathrm{d}} = \theta(\lambda_{\mathrm{d}}, c_{\mathrm{T,d}}). \tag{7}$$

Finally, the desired generator torque $M_{\mathrm{G,d}}$ can be obtained using (1a) and (2a):

$$M_{\mathrm{G,d}} = i_{\mathrm{GB}} \frac{1}{2} \rho\pi R^3 \frac{c_{\mathrm{P}}(\lambda_{\mathrm{d}}, \theta_{\mathrm{d}})}{\lambda_{\mathrm{d}}} v_0^2. \tag{8}$$

If the generator torque and pitch angle of the SLOW model follow the desired values $M_{\mathrm{G,d}}$ and θ_{d}, the rotor and tower motions are unaffected by changing wind speed v_0. To visualize the control action, $M_{\mathrm{G,d}}$ and θ_{d} are calculated for the operating point at $v_{\mathrm{op}} = 12\,\mathrm{m/s}$ and for wind speeds with $\pm 0.5\,\mathrm{m/s}$ and are plotted in Figure 4.

In the second step, $M_{\mathrm{G,d}}$ and θ_{d} are approximated by linear functions in v_0 with regression coefficients $a_{\mathrm{G}}, b_{\mathrm{G}}, a_{\mathrm{P}}$, and b_{P}:

$$M_{\mathrm{G,d}} \approx a_{\mathrm{G}} + b_{\mathrm{G}}\ (v_0 - v_{\mathrm{op}}) \tag{9a}$$

$$\theta_{\mathrm{d}} \approx a_{\mathrm{P}} + b_{\mathrm{P}}\ (v_0 - v_{\mathrm{op}}). \tag{9b}$$

In the third step, the feedforward actions are combined with the feedback controller in region 2.5 as depicted in Figure 3. A generator torque rate updated is added to the integral term of the torque feedback controller similar to the collective pitch rate update used in [1]-[4]:

$$\dot{M}_{\mathrm{G,FF}} = b_{\mathrm{G}}\ \dot{v}_0. \tag{10}$$

Performing the same for the pitch angle would not have the desired effect, since the integrator of the PI pitch controller will have negative values in region 2.5. Therefore, a feedforward updated to the minimal pitch angle $\theta_{\min}$ is used:

$$\Delta\theta_{\mathrm{FF}} = b_{\mathrm{P}}\ (v_0 - \bar{v}_0), \tag{11}$$

where $\bar{v}_0$ is a low pass filtered value of v_0 to account for changing wind speeds and to avoid excessive pitch action in region 2.5. Here, a first-order linear filter with a cutoff frequency of $f_{\mathrm{on}} = 0.01\,\mathrm{Hz}$ is used. The filter allows slow movements of the tower and thus fulfills a similar role to the tower trajectory planning of the flatness-based controller. However, the next section will show, that the tuning of f_{on} is more intuitive compared to the trajectory planning. A low pass filter is used instead of a high pass filter, because $\bar{v}_0$ can be calculated from the wind preview before shifting it in time and thus less phase delay is achieved. Additionally, in a future work $\bar{v}_0$ can be used to adjust the minimum pitch angle $\theta_{\min}$ as proposed in [19] and to schedule b_{P}, if necessary.

The feedforward controller might be derived directly from a linearized model with a similar outcome. Here, the relationship to the flatness-based controller is pointed out.

D. Adjustment for Realistic Wind Preview

Using a lidar system, the rotor-effective wind speed v_0 cannot be measured perfectly as discussed in Section III. While in [20] the measurement coherence is directly included in the control design, a prefilter is here used in addition to the controller. Previous work showed, that the transfer function between $v_{0\mathrm{L}}$ and v_0 is the optimal prefilter for the lidar estimate to remove all uncorrelated frequencies [21], [16]. A first-order low pass filter with a cut-off frequency of $f_{\mathrm{off}} = 0.134\,\mathrm{Hz}$ is fitted to the transfer function.

V. Simulation Results

In this section, the multivariable feedforward controller is evaluated by simulations first using perfect wind preview and then using simulated lidar measurements.

A. Simulations Using Perfect Wind Preview

In a first simulation study, the feedforward controller is tested assuming perfect wind preview to verify that the design objectives (less rotor and less tower motion) can be achieved for the full simulation model.

Therefore, the full aero-elastic model is disturbed by a coherent gust at 12 m/s similar to [22], but only with 1 m/s amplitude (minimum to maximum) to stay within region 2.5. The proposed feedforward controller can achieve almost perfect cancellation of the effect from v_0 to Ω and x_{T}, see Figure 5. The overshoot of the rotor speed (deviation from $\Omega_{\mathrm{rated}} = 12.1\,\mathrm{rpm}$) can be reduced by $95.9\,\%$ and the maximum tower base fore-aft bending moment $M_{y\mathrm{T}}$ by $10.9\,\%$ compared to the feedback controller, see Table I.

TABLE I

Maximum values of simulation with perfect wind preview.

	FB	FB+FF	$\frac{\text{FB+FF}}{\text{FB}}$ [%]
$\Delta\Omega$ [rpm]	0.203	0.008	4.1
$M_{y\mathrm{T}}$ [MNm]	79.4	70.7	89.1

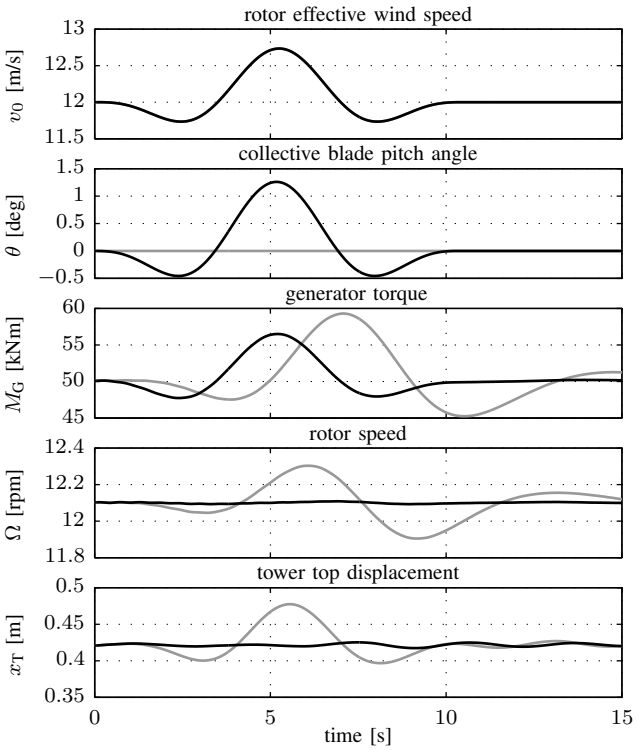

Fig. 5. Reaction to a small gust at 12 m/s with perfect wind preview. Feedback controller only (gray) and with additional feedforward (black).

The proposed feedforward controller demonstrates a good robustness against model uncertainties. Although the controller is designed with a nonlinear model with only two DOFs (rotor and tower motion) and static aerodynamics, it is able to almost perfectly cancel out the effect from the rotor-effective wind to the rotor speed and tower displacement for a full aero-elastic model with 15 DOFs. Thus, the results are consistent with the control objectives.

B. Simulations Using Simulated Lidar Measurements

In a second simulation study, the robustness against wind measurement errors of the simulated lidar system is examined. For this investigation, a turbulent wind field with a mean wind speed of $\bar{u} = 12\,\mathrm{m/s}$, a very low turbulence intensity ($7\,\%$) and a length of over 1 h is generated using TurbSim. The low turbulence is chosen to stay in region 2.5, which helps to isolate and to better understand the benefit of the proposed feedforward controller.

Figure 6 illustrates a representative 5 min period of the simulation. In the top part of the figure, the time shift and

a good agreement between the rotor-effective wind speed from the wind field and its lidar estimate can be observed. Due to the limitations of the lidar measurements and the not exact preview, a perfect performance similar to the previous section cannot be expected. However, with this more realistic wind preview, the variations in the rotor speed Ω and tower top displacement x_T are still reduced significantly. The effect of the multivariable feedforward controller in the frequency domain is visible in the Power Spectral Densities (PSDs) in Figure 7. The multivariable feedforward controller can significantly reduce the influence of the wind disturbance to the rotor speed at low frequencies, mainly by the generator torque rate update. Since the adaptive filter has a cut-off-frequency at $f_\mathrm{off} = 0.134\,\mathrm{Hz}$, the improvement minimizes above this frequency and no reduction is achieved at the damped eigenfrequency of the tower ($0.322\,\mathrm{Hz}$) and the $3P$ (three-times-per-revolution) frequency ($0.601\,\mathrm{Hz}$). In addition, the spectrum of the generator torque is reduced at low frequencies. This effect is similar to the collective pitch feedforward controller, where less pitch action is necessary to reduce the rotor speed variation. The tower base fore-aft bending moment is also significantly reduced for low frequencies up to f_off. However, the reduction starts at $f_\mathrm{on} = 0.01\,\mathrm{Hz}$, since by (11) and the used low pass filter, pitch actions below this frequency are hindered.

Finally, Table II summarizes the results of the 1 h simulation at 12 m/s. Over 55 % reduction in the standard deviation of the rotor speed can be achieved. For the calculation of the Damage Equivalent Loads (DELs), a reference number of cycles 2×10^6 is used. Further, a Wöhler exponent of 4 is assumed for the fatigue load calculation of the tower base fore-aft bending moment $M_{y\mathrm{T}}$ and the low-speed shaft torque M_LSS. For M_oop1, the out-of-plane blade root bending moment of blade 1, a Wöhler exponent of 10 is applied. Besides the load reduction on the tower base (15 %), additional load reductions on shaft and blade root (6 % and 5 %, respectively) are achieved. Taking into account the low turbulence intensity, the load reduction is promising.

The improvements come with some worsening. The increase in pitch activity (represented by the standard deviation of the pitch rate) in considered to be not relevant, because in full load operation, the pitch rate is more than ten times larger [15]. However, the loss in energy production (EP) of 0.14 % is not insignificant. However, using both the multivariable feedforward and the adjustments of the minimum pitch angle might result in load reduction and increase in energy production. Figure 8 shows the power coefficient c_P at $v_0 = 12\,\mathrm{m/s}$ and $\Omega = \Omega_\mathrm{rated}$ (resulting in $\lambda = 6.65$). By changing the minimum pitch angle θ_min from 0 deg to -1 deg, the power coefficient can be increased by 0.66 %. The optimal minimum pitch angle changes with the mean wind speed and the benefit is increasing closer to region 3 [19]. Thus, it can be expected that lidar measurements can be used to adjust θ_min and to increase the energy production even above the aforementioned losses.

TABLE II

RESULTS FOR THE 1 h SIMULATION WITH TURBULENT WIND.

	FB	FB+FF	$\frac{\text{FB+FF}}{\text{FB}}$ [%]
STD(Ω) [rpm]	0.0346	0.0154	44.6
DEL($M_{y\mathrm{T}}$) [MNm]	24.0	20.2	84.3
DEL(M_LSS) [MNm]	2.64	2.47	93.7
DEL(M_oop1) [MNm]	5.76	5.50	95.4
STD($\dot{\theta}$) [deg/s]	0	0.0702	∞
EP [MWh]	5.663	5.655	99.9

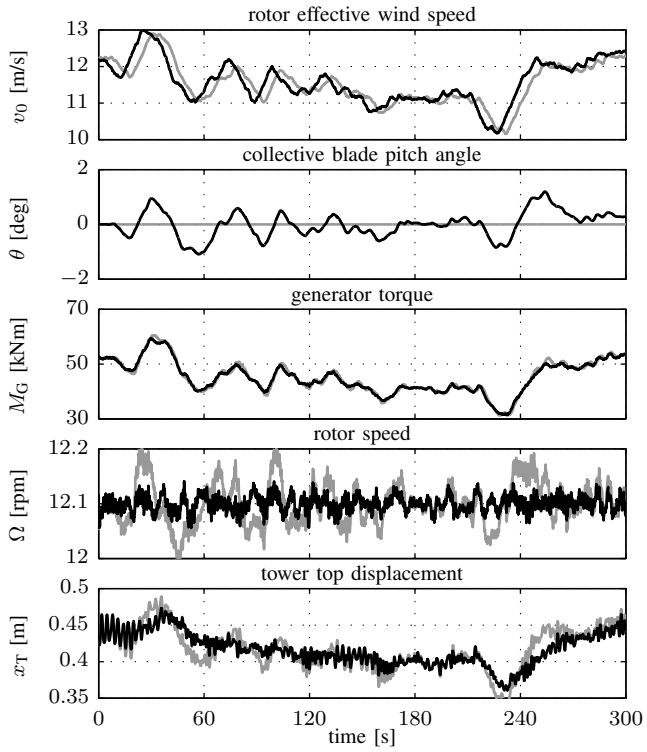

Fig. 6. Reaction to a turbulent wind field. Top: rotor-effective wind speed (gray) and its lidar estimate (black). Rest: Feedback controller only (gray) and with additional feedforward (black) using simulated lidar measurements.

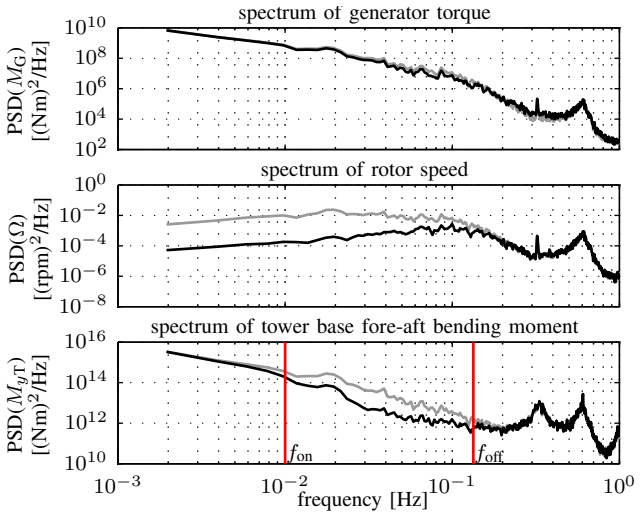

Fig. 7. PSDs for the 1 h simulation: Feedback controller only (gray) and with additional feedforward (black). Corner frequencies of used filters (red).

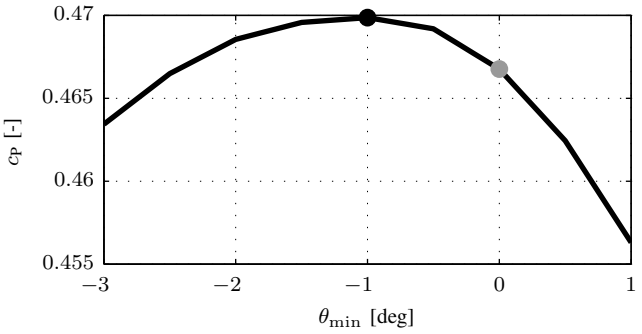

Fig. 8. Power coefficient at 12 m/s and rated rotor speed. By changing the minimum pitch angle from 0 deg (gray) to −1 deg (black), the power coefficient can be increased from 0.4668 to 0.4699 (0.66 %).

VI. Conclusions and Outlook

This paper presents a multivariable feedforward controller for wind turbines using lidar. The feedforward controller is designed to assist conventional feedback controllers for generator torque and collective pitch angle in the transition between partial to full load operations. The design is based on a flatness-based approach presented in previous work, but is simplified by a linearization and adjusted to avoid large pitch actions caused by large mean wind speed changes. Additionally, a PI generator torque controller is designed for the 5 MW reference wind turbine. The transition region is extended by increasing the rated power to 8 MW in order to have a sufficient large range for testing the concept.

Simulations with a full aero-elastic model and coherent wind show that the combined feedback-feedforward controller follows the design objectives and is able to keep rotor speed and tower motion constant assuming perfect wind preview. Promising load reduction is achieved in simulations with turbulent wind and a lidar simulator. The energy production is also slightly decreased, but possibilities to avoid the loss or even improve the energy production are outlined.

For future work, the following points are pursued:

- Design of a full feedback controller including a tower and drive train damper for the 8 MW wind turbine.
- Design a strategy to smoothly enable and disable the multivariable feedforward controller when entering and leaving the region 2.5 and to combine it with the collective pitch feedforward controller.
- Include the adjustment of the minimum pitch angle based on the lidar measurements as proposed in [19].
- Test the proposed multivariable controller in a detailed load analysis with a higher turbulence level.
- Determine the overall effect on energy production and load reduction of the concept.
- If the benefits can be further confirmed, a field testing on a real turbine is pursued.

Acknowledgments

The author would like to thank Paul Fleming and Na Wang from NREL, Lucy Pao from CU Boulder, Holger Fürst, Florian Haizmann, and Steffen Raach from the SWE control group for the helpful discussions.

References

[1] A. Scholbrock, P. Fleming, L. Fingersh, A. Wright, D. Schlipf, F. Haizmann, and F. Belen, "Field testing LIDAR based feed-forward controls on the NREL controls advanced research turbine," in *Proceedings of the 51st AIAA Aerospace Sciences Meeting Including the New Horizons Forum and Aerospace Exposition*, Dallas, USA, 2013.

[2] D. Schlipf, P. Fleming, F. Haizmann, A. Scholbrock, M. Hofsäß, A. Wright, and P. W. Cheng, "Field testing of feedforward collective pitch control on the CART2 using a nacelle-based lidar scanner," *Journal of Physics: Conference Series*, vol. 555, no. 1, p. 012090, 2014.

[3] D. Schlipf, P. Fleming, S. Raach, A. Scholbrock, F. Haizmann, R. Krishnamurthy, M. Boquet, A. Wright, and P. W. Cheng, "An adaptive data processing technique for lidar-assisted control to bridge the gap between lidar systems and wind turbines," in *EWEA 2015 Conference Proceedings In Press*, Paris, France, November 2015.

[4] A. Kumar, E. A. Bossayni, A. K. Scholbrock, P. A. Fleming, M. Boquet, and R. Krishnamurthy, "Field testing of lidar assisted feedforward control algorithms for improved speed control and fatigue load reduction on a 600 kW wind turbine," in *EWEA 2015 Conference Proceedings In Press*, Paris, France, November 2015.

[5] D. Schlipf, P. Fleming, S. Kapp, A. Scholbrock, F. Haizmann, F. Belen, A. Wright, and P. W. Cheng, "Direct speed control using lidar and turbine data," in *Proceedings of the American Control Conference*, Washington, USA, 2013.

[6] E. Bossanyi, A. Kumar, and O. Hugues-Salas, "Wind turbine control applications of turbine-mounted lidar," *Journal of Physics: Conference Series*, vol. 555, no. 1, p. 012011, 2014.

[7] D. Schlipf, L. Y. Pao, and P. W. Cheng, "Comparison of feedforward and model predictive control of wind turbines using LIDAR," in *Proceedings of the Conference on Decision and Control*, Maui, USA, 2012.

[8] A. Körber and R. King, "Nonlinear model predictive control for wind turbines," in *Proceedings of the European Wind Energy Association annual event*, Brussels, Belgium, 2011.

[9] S. Gros, "An economic nmpc formulation for wind turbine control," in *Proceedings of the Conference on Decision and Control*, Florence, Italy, 2013.

[10] D. Schlipf and P. W. Cheng, "Flatness-based feedforward control of wind turbines using lidar," in *Proceedings of the 19th World Congress of the International Federation of Automatic Control*, Cape Town, South Africa, 2014.

[11] J. Jonkman, S. Butterfield, W. Musial, and G. Scott, "Definition of a 5-MW reference wind turbine for offshore system development," NREL, Tech. Rep. TP-500-38060, February 2009.

[12] J. Jonkman and M. L. Buhl, "FAST user's guide," NREL, Tech. Rep. EL-500-38230, August 2005.

[13] B. J. Jonkman, "TurbSim user's guide," NREL, Tech. Rep. TP-500-46198, September 2009.

[14] T. Burton, N. Jenkins, D. Sharpe, and E. Bossanyi, *Wind Energy Handbook*. New York, USA: John Wiley & Sons, 2011.

[15] D. Schlipf, "Lidar-assisted control concepts for wind turbines," Ph.D. dissertation, University of Stuttgart, 2015.

[16] D. Schlipf, F. Haizmann, N. Cosack, T. Siebers, and P. W. Cheng, "Detection of wind evolution and lidar trajectory optimization for lidar-assisted wind turbine control," *Meteorologische Zeitschrift*, vol. 24, no. 6, pp. 565–579, 11 2015.

[17] E. A. Bossanyi, "The design of closed loop controllers for wind turbines," *Wind Energy*, vol. 3, no. 3, pp. 149–163, 2000.

[18] M. H. Hansen, A. Hansen, T. J. Larsen, S. Oye, P. Sorensen, and P. Fuglsang, "Control design for a pitch-regulated, variable speed wind turbine," Riso National Laboratory, Tech. Rep. Riso-R-1500(EN), 2005.

[19] N. Wang, K. Johnson, A. Wright, and C. Carcangiu, "Lidar-assisted preview controllers design for a MW-scale commercial wind turbine model," in *Decision and Control (CDC), 2013 IEEE 52nd Annual Conference on*, Dec 2013, pp. 1678–1683.

[20] F. Dunne and L. Y. Pao, "Benefit of wind turbine preview control as a function of measurement coherence and preview time," in *Proceedings of the American Control Conference*, Washington, USA, 2013.

[21] E. Simley and L. Y. Pao, "Reducing lidar wind speed measurement error with optimal filtering," in *Proceedings of the American Control Conference*, Washington, USA, 2013.

[22] IEC 61400-1, *Wind turbines - Part 1: Design requirements*, International Electrotechnical Commission Std., Rev. third edition, 2005.